Eur. Phys. J. C (2008) 56: 493–510
DOI 10.1140/epjc/s10052-008-0671-x

THE EUROPEAN PHYSICAL JOURNAL C

Regular Article - Theoretical Physics

The thermal production of strange and non-strange hadrons in e^+e^- collisions

F. Becattini[1], **P. Castorina**[2], **J. Manninen**[3], **H. Satz**[4,a]

[1]Dipartimento di Fisica, Università di Firenze, and INFN Sezione di Firenze, 50019 Sesto Fiorentino (Firenze), Italy
[2]Dipartimento di Fisica, Università di Catania, and INFN Sezione di Catania, 95123 Catania, Italy
[3]INFN Sezione di Firenze, 50019 Sesto Fiorentino (Firenze), Italy
[4]Fakultät für Physik, Universität Bielefeld, 33615 Bielefeld, Germany

Received: 16 May 2008 / Published online: 5 August 2008

Abstract The thermal multihadron production observed in different high energy collisions poses two basic problems. (1) Why do even elementary collisions with comparatively few secondaries (e^+e^- annihilation) show thermal behavior? (2) Why is there in such interactions a suppression of strange particle production? We show that the recently proposed mechanism of thermal hadron production through Hawking–Unruh radiation can naturally account for both. The event horizon of color confinement leads to thermal behavior, but the resulting temperature depends on the strange quark content of the produced hadrons, causing a deviation from full equilibrium and hence a suppression of strange particle production. We apply the resulting formalism to multihadron production in e^+e^- annihilation over a wide energy range and make a comprehensive analysis of the data in the conventional statistical hadronization model and the modified Hawking–Unruh formulation. We show that this formulation provides a very good description of the measured hadronic abundances, fully determined in terms of the string tension and the bare strange quark mass; it contains no adjustable parameters.

1 Introduction

Hadron production in high energy collisions shows remarkably universal thermal features. In e^+e^- annihilation [1–3], in pp, $p\bar{p}$ [4] and more general hh interactions [3], as well as in the collisions of heavy nuclei [5–11], over an energy range from around 10 GeV up to the TeV range, the relative abundances of the produced hadrons appear to be those of an ideal hadronic resonance gas at a quite universal temperature $T_H \approx 160$–170 MeV, as illustrated in Fig. 1 [12]. The transverse momentum spectra of the hadrons produced in hadronic collisions at intermediate energies are also in good agreement with the predictions of a statistical model based on the same temperature [3].

There is, however, one important non-equilibrium effect observed: the production of strange hadrons in elementary collisions is suppressed relative to overall equilibrium. This is usually taken into account phenomenologically by introducing an overall strangeness suppression factor $\gamma_s < 1$ [13], which reduces the predicted abundances by γ_s, γ_s^2 and γ_s^3 for hadrons containing one, two or three strange quarks (or antiquarks), respectively. In high energy heavy ion colli-

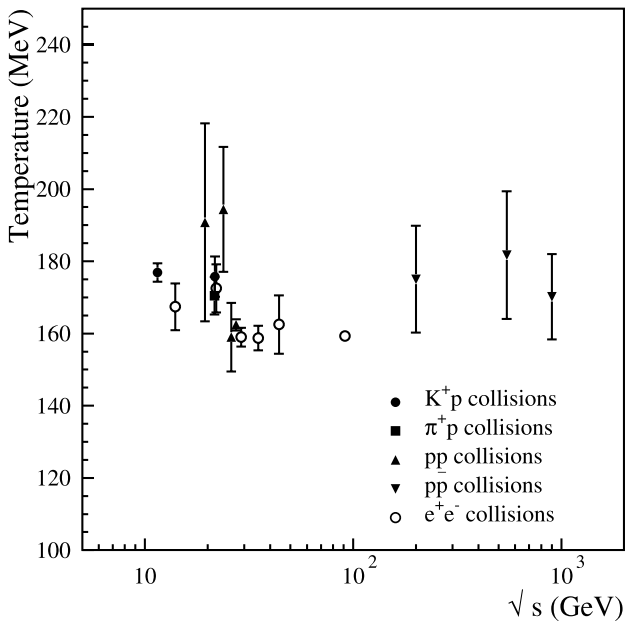

Fig. 1 Hadronization temperatures [12]

[a] e-mail: satz@physik.uni-bielefeld.de

sions, strangeness suppression becomes less and disappears at high energies [14, 15].

When comparing the temperatures of different collision channels in Fig. 1, it should be stressed that in elementary collisions, in contrast to heavy ion collisions, the conservation of charge, baryon number and strangeness is enforced exactly (canonical ensemble), so that here no chemical potential is introduced. The effect of exact charge conservation is important in elementary collisions because of the low multiplicities involved, while it is generally negligible in large multiplicity high energy nuclear reactions. The fit values of γ_s lie around 0.5 to 0.7 in elementary collisions; the heavy ion values appear to vary as a function of energy but tend to approach unity [14, 15].

The origin of the observed thermal behavior has been an enigma for many years, and there is still ongoing debate about the interpretation of these results [16–24]. While the common belief is that in high energy heavy ion collisions multiple parton scattering could lead to kinetic thermalization through multiple scattering, e^+e^- or elementary hadron interactions do not readily allow such a description. The universality of the observed temperatures, on the other hand, suggests a common origin for all high energy collisions, and it was recently proposed [25] that thermal hadron production is the QCD counterpart of Hawking–Unruh radiation [26, 27], emitted at the event horizon due to color confinement. A well-known instance of this phenomenon is the Schwinger mechanism [28–33] of pair production in a constant electric field $\mathcal{E}$. The probability of spontaneously producing an electron-positron pair is in this case given by

$$P(m.\mathcal{E}) \sim \exp\{-\pi m^2/e\mathcal{E}\}, \tag{1}$$

where m is the electron mass and e its charge. Since

$$a_e = \frac{2e\mathcal{E}}{m} \tag{2}$$

is just the acceleration of an electron (of reduced mass $m/2$) in the field $\mathcal{E}$, we find that the pair production probability has the thermal form,

$$P(m,\mathcal{E}) \sim \exp\{-m/T_U\}, \tag{3}$$

where

$$T_{\mathrm{U}} = \frac{a_e}{2\pi} = \frac{e\mathcal{E}}{\pi m} \tag{4}$$

is the corresponding temperature. In other words, it is just that obtained by Unruh [27] for the radiation emitted when a mass suffers constant acceleration and hence encounters an event horizon.

In the case of QCD and approximately massless quarks, the resulting hadronization temperature is determined by the string tension σ, with $T \simeq \sqrt{\sigma/2\pi}$. The aim of the present work is to show that strangeness suppression occurs naturally in this framework, without requiring a specific suppression factor. The crucial role here is played by the non-negligible strange quark mass, which modifies the emission temperature for such quarks.

In this work, we will focus on e^+e^- collisions, which is the simplest case for this model to be tested. In the next section, we will briefly review the usual formulation of the statistical hadronization model, since this will form the basis also for the subsequent description in terms of the Hawking–Unruh radiation model, to be formulated in Sect. 3. There we shall in particular derive the dependence of the radiation temperature on the mass of the produced quark and show how this affects the hadronization in e^+e^- annihilation. In Sect. 4, we present an updated comprehensive analysis of all available data from $\sqrt{s} = 14$ GeV to $\sqrt{s} = 189$ GeV and compare the results of the Hawking–Unruh formulation to the conventional statistical description.

2 Statistical hadronization in e^+e^- collisions

In this section we will briefly review the essentials of the statistical hadronization model and its application to e^+e^- collisions. For a detailed description, see Ref. [34].

The statistical hadronization model assumes that hadronization in high energy collisions is a universal process proceeding through the formation of multiple colorless massive clusters (or fireballs) of finite spatial extension. These clusters are taken to decay into hadrons according to a purely statistical law: every multihadron state of the cluster phase space defined by its mass, volume and charges is equally probable. The mass distribution and the distribution of charges (electric, baryonic and strange) among the clusters and their (fluctuating) number are determined in the prior dynamical stage of the process. Once these distributions are known, each cluster can be hadronized on the basis of statistical equilibrium, leading to the calculation of averages in the *microcanonical ensemble*, enforcing the exact conservation of energy and charges of each cluster.

Hence, in principle, one would need the mentioned dynamical information in order to make definite quantitative predictions to be compared with data. Nevertheless, for Lorentz-invariant quantities such as multiplicities, one can introduce a simplifying assumption and thereby obtain a simple analytical expression in terms of a temperature. The key point is to assume that the distribution of masses and charges among clusters is again purely statistical [3], so that, as far as the calculation of multiplicities is concerned, the set of clusters becomes equivalent, on average, to a large

cluster (*equivalent global cluster*) whose volume is the sum of proper cluster volumes and whose charge is the sum of cluster charges (and thus the conserved charge of the initial colliding system). In such a global averaging process, the equivalent cluster generally turns out to be large enough in mass and volume so that the canonical ensemble becomes a good approximation of the more fundamental microcanonical ensemble [35, 36]; in other words, a temperature can be introduced which replaces the a priori more fundamental description in terms of an energy density.

It should be stressed that in such an analysis of multiplicities, temperature has essentially a global meaning and not a local meaning as in hydrodynamical models. The only local meaningful quantity is the cluster's energy density, and even though the globally fit temperature value is closely related to it, this does not mean that single physical clusters can be described in terms of a temperature, unless they are sufficiently large (about 10 GeV in mass, see [35]).

In the statistical hadronization model supplemented by global cluster averaging, the primary multiplicity of each hadron species j is given by [3]

$$\langle n_j\rangle^{\text{primary}} = \frac{VT(2J_j+1)}{2\pi^2}\sum_{n=1}^{\infty}\gamma_s^{N_s n}(\mp 1)^{n+1}\frac{m_j^2}{n} \times \mathrm{K}_2\left(\frac{nm_j}{T}\right)\frac{Z(\mathbf{Q}-n\mathbf{q}_j)}{Z(\mathbf{Q})} \tag{5}$$

where V is the (mean) volume and T the temperature of the equivalent global cluster. Here $Z(\mathbf{Q})$ is the canonical partition function depending on the initial Abelian charges $\mathbf{Q} = (Q, N, S, C, B)$, i.e., electric charge, baryon number, strangeness, charm and beauty, respectively. We denote by m_j and J_j the mass and the spin of the hadron j, and $\mathbf{q}_j = (Q_j, N_j, S_j, C_j, B_j)$ its corresponding charges; γ_s is the extra phenomenological factor implementing a suppression of hadrons containing N_s strange valence quarks (see Sect. 1). In the sum (5), the upper sign applies to bosons and the lower sign to fermions. For temperature values of 160 MeV or higher, Boltzmann statistics corresponding to the term $n = 1$ only in the series (5) is a very good approximation for all hadrons (within 1.5%) but pions. For resonances, (5) is folded with a relativistic Breit–Wigner distribution of the mass m_j.

The canonical partition function can be expressed as a multi-dimensional integral

$$Z(\mathbf{Q}) = \frac{1}{(2\pi)^N}\int_{-\pi}^{+\pi}\mathrm{d}^N\phi\,\mathrm{e}^{\mathrm{i}\mathbf{Q}\cdot\phi} \times\exp\left[\frac{V}{(2\pi)^3}\sum_j(2J_j+1) \times\int\mathrm{d}^3p\log\left(1\pm\gamma_s^{N_{sj}}\mathrm{e}^{-\sqrt{p^2+m_j^2}/T_i-\mathrm{i}\mathbf{q}_j\cdot\phi}\right)^{\pm 1}\right] \tag{6}$$

where N is the number of conserved Abelian charges. Unlike the grand-canonical case, the logarithm of the canonical partition function does not scale linearly with the volume. Therefore, the chemical factors $Z(\mathbf{Q}-n\mathbf{q}_j)/Z(\mathbf{Q})$ turn out to be less than unity at finite volume (canonical suppression) and only asymptotically reach their grand-canonical limit of unity, for an initially completely neutral system. Indeed, they play a major role in determining particle yields in e^+e^- collisions.

For all energies considered here, the production of heavy-flavored hadrons is negligible in $e^+e^- \to q\bar{q}$ events, where q is a light quark (u, d, s). As a result, in (5) the charm and bottom charge can be neglected, so that the Abelian charge vector reduces to a three-component form $\mathbf{Q} = (Q, N, S)$ and can be calculated with a numerical integration [4, 37]. On the other hand, $e^+e^- \to q\bar{q}$ events, where q is a heavy quark, always result in the production of two open heavy-flavored hadrons, arising from the primary heavy quark–antiquark pair, which subsequently decay into light-flavored hadrons. In the statistical model, this constraint is readily implemented, requiring the number of heavy quarks plus antiquarks in the global description to be two; because of the high charm/bottom mass compared to the typical temperature value of 160 MeV, the probability of producing extra heavy $q\bar{q}$ pairs is absolutely negligible. The multiplicities of charm (bottom) hadrons in $e^+e^- \to c\bar{c}$ $(e^+e^- \to b\bar{b})$ events become in the Boltzmann approximation [2, 4]

$$\langle n_j\rangle = \gamma_s^{N_{Sj}} z_j\frac{\sum_i\gamma_s^{N_{si}} z_i\zeta(\mathbf{Q}-\mathbf{q}_j-\mathbf{q}_i)}{\sum_{i,k}\gamma_s^{N_{si}}\gamma_s^{N_{sk}} z_i z_k\zeta(\mathbf{Q}-\mathbf{q}_i-\mathbf{q}_k)}, \tag{7}$$

where

$$z_j = \frac{V}{2\pi^2}(2J_j+1)m_j^2 T\mathrm{K}_2\left(\frac{m_j}{T}\right), \tag{8}$$

and ζ denotes the canonical partition function as in (6), involving only light-flavored particles, with $N = 3$. The indices j and k label charm (bottom) hadrons, while the index i labels their antiparticles.

The statistical treatment of heavy quark formation and hadronization as outlined here effectively means that heavy quarks occur only in $e^+e^- \to q\bar{q}$ interactions, leading to one open charm (bottom) hadron and one corresponding antihadron per event. The relative rates of the different possible open charm (bottom) states, however, are determined by their phase space weights.

3 String breaking and event horizons

We first outline the thermal hadron production process through Hawking–Unruh radiation for the specific case of

e^+e^- annihilation (see Fig. 2). The separating primary $q\bar{q}$ pair excites a further pair $q_1\bar{q}_1$ from the vacuum, and this pair is in turn pulled apart by the primary constituents. In the process, the $\bar{q}_1$ shields the q from its original partner $\bar{q}$, with a new $q\bar{q}_1$ string formed. When it is stretched to reach the pair production threshold, a further pair is formed, and so on [38, 39]. Such a pair production mechanism is a special case of Hawking–Unruh radiation [29–33], emitted as hadron $\bar{q}_1 q_2$ when the quark q_1 tunnels through its event horizon to become $\bar{q}_2$. The corresponding hadron radiation temperature is given by the Unruh form $T_H = a/2\pi$, where a is the acceleration suffered by the quark $\bar{q}_1$ due to the force of the string attaching it to the primary quark Q. This is equivalent to that suffered by quark q_2 due to the effective force of the primary antiquark $\bar{Q}$. Hence, we have

$$a_q = \frac{\sigma}{w_q} = \frac{\sigma}{\sqrt{m_q^2 + k_q^2}}, \tag{9}$$

where $w_q = \sqrt{m_q^2 + k_q^2}$ is the effective mass of the produced quark, with m_q for the bare quark mass and k_q the quark momentum inside the hadronic system $q_1\bar{q}_1$ or $q_2\bar{q}_2$. Since the string breaks [25] when it reaches a separation distance

$$x_q \simeq \frac{2}{\sigma}\sqrt{m_q^2 + (\pi\sigma/2)}, \tag{10}$$

the uncertainty relation gives us, with $k_q \simeq 1/x_q$,

$$w_q = \sqrt{m_q^2 + \left[\sigma^2/(4m_q^2 + 2\pi\sigma)\right]} \tag{11}$$

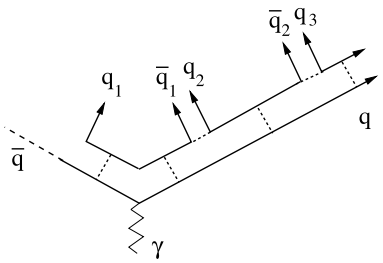

Fig. 2 String breaking through $q\bar{q}$ pair production

for the effective mass of the quark. The resulting quark-mass-dependent Unruh temperature is thus given by

$$T(qq) \simeq \frac{\sigma}{2\pi w_q}. \tag{12}$$

Note that here it is assumed that the quark masses for q_1 and q_2 are equal. For $m_q \simeq 0$, (12) reduces to

$$T(00) \simeq \sqrt{\frac{\sigma}{2\pi}}, \tag{13}$$

as obtained in [25].

If the produced hadron $\bar{q}_1 q_2$ consists of quarks of different masses, the resulting temperature has to be calculated as an average of the different accelerations involved. For one massless quark ($m_q \simeq 0$) and strange quark mass m_s, the average acceleration becomes

$$\bar{a}_{0s} = \frac{w_0 a_0 + w_s a_s}{w_0 + w_s} = \frac{2\sigma}{w_0 + w_s}. \tag{14}$$

From this, the Unruh temperature of a strange meson is given by

$$T(0s) \simeq \frac{\sigma}{\pi(w_0 + w_s)}, \tag{15}$$

with $w_0 \simeq \sqrt{1/2\pi\sigma}$. Similarly, we obtain

$$T(ss) \simeq \frac{\sigma}{2\pi w_s}, \tag{16}$$

for the temperature of a meson consisting of a strange quark–antiquark pair (ϕ). With $\sigma \simeq 0.2$ GeV^2, (13) gives $T_0 \simeq 0.178$ GeV. A strange quark mass of 0.1 GeV reduces this to $T(0s) \simeq 0.167$ GeV and $T(ss) \simeq 157$ MeV, i.e., by about 6% and 12%, respectively.

The scheme is readily generalized to baryons. The production pattern is illustrated in Fig. 3 and leads to an average of the accelerations of the quarks involved. We thus have

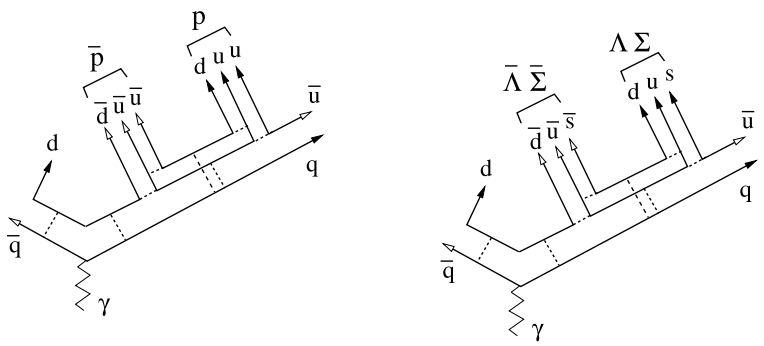

Fig. 3 Nucleon (*left*) and hyperon (*right*) production in e^+e^- annihilation

$$T(000) = T(0) \simeq \frac{\sigma}{2\pi w_0} \tag{17}$$

for nucleons,

$$T(00s) \simeq \frac{3\sigma}{2\pi(2w_0 + w_s)} \tag{18}$$

for Λ and Σ production,

$$T(0ss) \simeq \frac{3\sigma}{2\pi(w_0 + 2w_s)} \tag{19}$$

for Ξ production, and

$$T(sss) = T(ss) \simeq \frac{\sigma}{2\pi w_s} \tag{20}$$

for that of the Ω. We thus obtain a resonance gas picture with five different hadronization temperatures, as specified by the strangeness content of the hadron in question: $T(00) = T(000)$, $T(0s)$, $T(ss) = T(sss)$, $T(00s)$ and $T(0ss)$.

It is important to stress that, in this picture, the primary quarks produced directly in the annihilation are not related to Hawking–Unruh radiation, nor are the light quarks with which they eventually combine to hadronize. Therefore, leading hadrons (those containing primary quarks) are essentially different and should be treated separately from hadrons containing only newly produced quarks. In practice, while in the conventional statistical model the same hadronization temperature governs the relative probabilities of emitting different species of leading hadrons, in the Hawking–Unruh formulation we do not have any specific prescription for this. The problem of calculating leading hadron yields is relevant in e^+e^- annihilations because, in contrast to hadronic collisions, the primary heavy quarks c and b have large branching ratios and significantly contribute to the production of light-flavored hadrons through the decay chain, especially in the strange sector. Lacking a definite recipe, we chose to calculate the relative heavy-flavored hadron yields by using the same temperatures as for the light-flavored ones, quoted above, keeping one weight w_0 fixed and using w_0 or w_s according to whether the heavy quark hadronization occurs through combination with either u, d or with s, respectively. It should be noted that this is not the only option and that different choices may lead to different results.

The different species-dependent temperatures are to be inserted into (5) and (7) of the previous section, in order to determine the primary hadron multiplicities. We note at this point a subtle conceptual difference between the conventional statistical approach and the Hawking–Unruh formulation. The usual statistical description employs, as noted above, a global cluster averaging, with each cluster statistically composed. In the Hawking–Unruh scheme, the radiation in each step is a hadron formed from the emitted $q\bar{q}$ pair, not some thermal cluster. Since the hadron can, however, be a highly excited resonance, the two descriptions become equivalent in a Hagedorn-type picture proposing resonances made up of resonances in a self-similar pattern.

Table 1 Hadronization temperatures for hadrons of different strangeness content, for $m_s = 0.075, 0.100, 0.125$ GeV and $\sigma = 0.2$ GeV^2

T	$m_s = 0.075$	$m_s = 0.100$	$m_s = 0.125$
$T(00)$	0.178	0.178	0.178
$T(0s)$	0.172	0.167	0.162
$T(ss)$	0.166	0.157	0.148
$T(000)$	0.178	0.178	0.178
$T(00s)$	0.174	0.171	0.167
$T(0ss)$	0.170	0.164	0.157
$T(sss)$	0.166	0.157	0.148

The multiplicities obtained in the Hawking–Unruh scheme are, as emphasized, fully determined by the two basic parameters of the formulation, the string tension σ and the strange quark mass m_s. Apart from possible variations of these quantities, our description is thus parameter free. As an illustration, we show in Table 1 the temperatures obtained for $\sigma = 0.2$ GeV^2 and three different strange quark masses. It is seen that in all cases, the temperature for a hadron carrying non-zero strangeness is lower than that of non-strange hadrons; as we shall show, this leads to an overall strangeness suppression.

Our picture implies that the produced hadrons are emitted slightly "out of equilibrium", in the sense that the emission temperatures are not identical. As long as there is no final state interference between the produced quarks or hadrons, we expect to observe this difference and hence a modification of the production of strange hadrons, in comparison to the corresponding full equilibrium values. Once such an interference becomes likely, as in high energy heavy ion collisions, equilibrium can be at least partially restored, weakening the strangeness suppression. The extension of our approach to heavy ion collisions will be dealt with in a subsequent paper.

4 Analysis of hadron multiplicities

Multihadron production in e^+e^- annihilation has been studied at PEP, PETRA and LEP over an energy range from 14 to 189 GeV, and the multiplicities of a large number of different species have been measured. The rele-

vant data and their references are compiled in the appendix.

In order to compare the models with the experimental data, we have at each energy made a fit to the available measured multiplicities of light-flavored hadrons, both in the traditional statistical model and in the Hawking–Unruh formulation. The traditional model has three free parameters to be determined, namely the temperature T, the global volume V (see the discussion in the Sect. 2), and the strangeness undersaturation parameter γ_s. In the Hawking–Unruh model, V is kept, but the string tension σ and the strange mass m_s replace T and γ_s as fit parameters.

In the fit, the theoretical multiplicity of a given species, to be compared to the data, is calculated as the sum of the primary multiplicity given by (5) and the contribution from the decay of unstable heavier hadrons,

$$\langle n_j \rangle = \langle n_i \rangle^{\text{primary}} + \sum_k \text{Br}(k \to j) \langle n_k \rangle, \tag{21}$$

where the branching ratios are the measured values as listed in the latest compilation of the Review of Particle Physics [40]. For the decays of heavy-flavored hadrons with unknown branching fractions, we have used the predictions of the PYTHIA [41] program. The hadrons considered unstable in e^+e^- experiments are all species except π, $K^\pm$, K^0_L, p, n, and we have followed this convention in the theoretical calculation to meet the definition of measured multiplicities. The hadrons and resonances contributing to the sum in (21) consist here of all known states [40] up to a mass of 1.8 GeV.

A specific fraction of e^+e^- annihilations occurs into heavy c and b quarks. In this case, the multiplicities of light-flavored hadrons are affected by the presence of the heavy quarks, both at primary level as the canonical partition function changes (see discussion in the previous section) and at final level because of the heavy-flavored hadron decays. This is taken into account in our calculations, and the production rate of the jth hadron is given by

$$\langle\langle n_j \rangle\rangle = \sum_{i=1}^{5} R_i \ \langle n_j \rangle_{q_i} \tag{22}$$

where $i = 1, \ldots, 5$ accounts for u, d, s, c, b quarks and the index q_i specifies the corresponding multiplicity in $e^+e^- \to q_i \bar{q}_i$ annihilation. The values of

$$R_i = \frac{\sigma(e^+e^- \to q_i \overline{q}_i)}{\sigma(e^+e^- \to \text{hadrons})} \tag{23}$$

are the corresponding branching fractions, obtained at each center-of-mass energy from measurements and electroweak calculations. We have here taken the values calculated in the PYTHIA program [41], which are quoted in Table 2 for each center-of-mass energy.

Table 2 Branching ratios for the $e^+e^- \to q\bar{q}$ annihilations into various quark flavors as a function of center-of-mass energy

$\sqrt{s}$	$R_u + R_d$	R_s	R_c	R_b
14	0.46	0.09	0.37	0.08
22	0.46	0.09	0.36	0.09
29	0.46	0.09	0.36	0.09
35	0.46	0.09	0.36	0.09
43	0.46	0.09	0.36	0.09
91.25	0.39	0.22	0.17	0.22
133	0.41	0.18	0.23	0.18
161	0.42	0.17	0.24	0.17
183	0.42	0.16	0.26	0.16
189	0.42	0.16	0.26	0.16

The mass of resonances with $\Gamma > 1$ MeV has been distributed according to a relativistic Breit–Wigner function over the interval $[m_0 - \Delta m, m_0 + \Delta m]$, m_0 where m_0 is the central mass value and $\Delta m = \min\{2\Gamma, m_0 - m_{\text{th}}\}$, Γ being the width and m_{th} the threshold mass value for the opening of all allowed decay channels. The primary production rate of neutral mesons such as η, η', ϕ, ω and others, which are a superposition of $s\bar{s}$ and $u\bar{u}$, $d\bar{d}$ states, has been suppressed with γ_s^2 according to the fraction of $s\bar{s}$ content. For this purpose, we use the mixing formulas quoted in the Review of Particles Properties [40] with angles $\theta = -10°$ and $\theta = 39°$ for the (η, η') system and for the (ω, ϕ) system, respectively, while for the other nonets we use $\theta = 28°$.

For each experiment, the most recent measurements have been considered. Multiple measurements from different experiments have been averaged according to the PDG method [40], with error rescaling in case of discrepancy; that is, a χ^2/dof of the weighted average >1. The overall calculated yields T_i are compared to the experimental measurements E_i, and the total overall χ^2,

$$\chi^2 = \sum_i (T_i - E_i)^2 / \sigma_i^2 \tag{24}$$

where σ_i are the experimental errors, is minimized. The minimization is in fact carried out in two steps, in order to take into account the uncertainties on input parameters, such as hadron masses, widths and branching ratios, according to the following procedure [3]. First a χ^2 with only experimental errors is minimized and preliminary best-fit model parameters are determined. Then, keeping the preliminary fit parameters fixed, the variations $\Delta n_j^{l\text{theo}}$ of the multiplicities corresponding to the variations of the l^{th} input parameter by one standard deviation are calculated. Such vari-

Table 3 Abundances of long-lived hadrons in e^+e^- collisions at $\sqrt{s} = 91.25$ GeV, compared to a statistical hadronization model fit based on T and γ_s. The third column shows the residual, defined as the difference between model and data divided by the error, while the fourth column shows the differences between model and data in percent. References to the original experimental publications can be found in Table 20 in the appendix

	Experiment (E)	Model (M)	Residual	$\lvert M - E\rvert/E$ [%]
π^0	9.61 ± 0.29	9.89	0.97	2.95
π^+	8.50 ± 0.10	8.48	−0.14	−0.167
K^+	1.127 ± 0.026	1.074	−2.0	−4.69
K^0_S	1.0376 ± 0.0096	1.0342	−0.35	−0.327
η	1.059 ± 0.086	1.020	−0.46	−3.72
ω	1.024 ± 0.059	0.993	−0.52	−2.99
p	0.519 ± 0.018	0.572	3.0	10.3
η'	0.166 ± 0.047	0.106	−1.3	−36.4
ϕ	0.0977 ± 0.0058	0.1163	3.2	19.0
Λ	0.1943 ± 0.0038	0.1846	−2.5	−4.98
Σ^+	0.0535 ± 0.0052	0.0429	−2.0	−19.9
Σ^0	0.0389 ± 0.0041	0.0435	1.1	11.8
Σ^-	0.0410 ± 0.0037	0.0391	−0.51	−4.58
Ξ^-	0.01319 ± 0.00050	0.01256	−1.3	−4.81
Ω	0.00062 ± 0.00010	0.00089	2.7	43.7

ations are considered as additional systematic uncertainties on the multiplicities and the following covariance matrix is formed,

$$\mathsf{C}^{\mathrm{sys}}_{ij} = \sum_l \Delta n^l_i \Delta n^l_j, \tag{25}$$

to be added to the experimental covariance matrix $\mathsf{C}^{\mathrm{exp}}$. Finally a new χ^2 is minimized with covariance matrix $\mathsf{C}^{\mathrm{exp}} + \mathsf{C}^{\mathrm{sys}}$, from which the best-fit estimates of the parameters and their errors are obtained. Actually, more than 350 among the most relevant or poorly known input parameters have been varied. However, it should be mentioned that no variation of the branching fractions of heavy-flavored hadrons has been done. Therefore, for some specific species, the systematic error could have been underestimated.

5 Results

5.1 Light-flavored hadrons

We begin our analysis with the most extensive sample, the LEP data at 91.25 GeV. It comes from a compilation of results from the four different experimental groups

Table 4 Abundances of long-lived hadrons in e^+e^- collisions at $\sqrt{s} = 91.25$ GeV, compared to a Hawking–Unruh fit in terms of string tension σ and strange quark mass m_s. The third column shows the residual, defined as the difference between model and data divided by the error, while fourth column shows the differences between model and data in percent. References to the original experimental publications can be found in Table 21 in the appendix

	Experiment (E)	Model (M)	Residual	$\lvert M - E\rvert/E$ [%]
π^0	9.61 ± 0.29	9.73	0.41	1.25
π^+	8.50 ± 0.10	8.32	−1.7	−2.06
K^+	1.127 ± 0.026	1.106	−0.80	−1.85
K^0_S	1.0376 ± 0.0096	1.0656	2.9	2.69
η	1.059 ± 0.086	1.006	−0.61	−4.98
ω	1.024 ± 0.059	0.967	−0.97	−5.58
p	0.519 ± 0.018	0.559	2.2	7.78
η'	0.166 ± 0.047	0.093	−1.6	−43.8
ϕ	0.0977 ± 0.0058	0.1057	1.4	8.11
Λ	0.1943 ± 0.0038	0.1892	−1.3	−2.63
Σ^+	0.0535 ± 0.0052	0.0438	−1.9	−18.2
Σ^0	0.0389 ± 0.0041	0.0444	1.4	14.2
Σ^-	0.0410 ± 0.0037	0.0401	−0.25	−2.22
Ξ^-	0.01319 ± 0.00050	0.01265	−1.1	−4.11
Ω	0.00062 ± 0.00010	0.00077	1.5	23.5

(see references at the end of the appendix), and it lists up to 30 different light-flavored species. However, for short-lived and hence broad resonances, the separation of resonance signal from background often becomes difficult, making the assessment of systematic errors problematic. Moreover, broad resonance yields are more sensitive to feeding from possibly unobserved heavier states or poorly known branching ratios. For this reason, we first consider, both for the conventional and for the Hawking–Unruh scenario, the analysis of the unproblematic ("golden") species of widths less than 10 MeV; this still leaves 15 different hadronic states to be analysed, listed in Tables 3 and 4.

As noted, the conventional statistical resonance gas approach is based on a universal temperature T, a strangeness suppression factor γ_s, and a global volume V. The fit of the long-lived species is shown in detail in Table 3 and Fig. 4 and the resulting fit parameters are

$$\begin{aligned} &T = 164.6 \pm 3.0 \text{ MeV}; \qquad \gamma_s = 0.648 \pm 0.026; \\ &V = 40.2 \pm 5.7 \text{ fm}^3, \end{aligned} \tag{26}$$

with a $\chi^2/\mathrm{dof} = 39/12$. The errors on the parameters are the fit errors rescaled by $\sqrt{\chi^2/\mathrm{dof}}$. Such a method [40] takes into account the additional uncertainty on the parameters if the fit leads to $\chi^2/\mathrm{dof} > 1$. This rescaling has been applied to all parameter errors quoted in this paper.

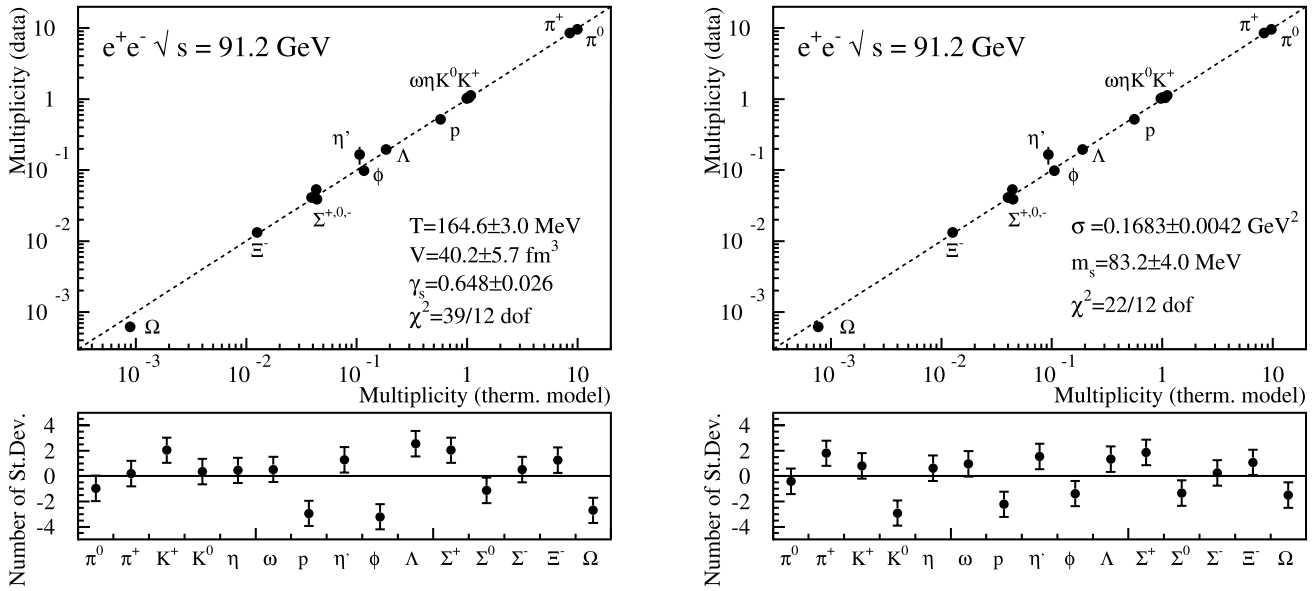

Fig. 4 Comparison between measured and fit multiplicities of long-lived hadronic species in e^+e^- collisions at $\sqrt{s} = 91.25$ GeV. *Left*: statistical hadronization model with one temperature. *Right*: Hawking–Unruh radiation model

Next, we perform the corresponding hadron-resonance gas analysis in the Hawking–Unruh formulation, introducing different temperatures determined by the string tension σ and the strange quark mass m_s. The results for long-lived species are shown in Table 4 and Fig. 4. The resulting fit parameters here are

$$\begin{aligned} &\sigma = 0.1683 \pm 0.0048\ \text{GeV}^2; \\ &m_s = 0.083 \pm 0.004\ \text{GeV}, \\ &V = 40.3 \pm 3.2\ \text{fm}^3; \end{aligned} \tag{27}$$

with a $\chi^2/\text{dof} = 22/12$, somewhat better than that of the corresponding conventional fit.

We now repeat both analyses using the entire 91.25 GeV data set, with the results shown in table XX and XXI of the appendix. The resulting fit values (see Tables 3 and 4) agree well within errors with those obtained from the "golden" data set at 91.25 GeV. As expected, because of the mentioned error sizes, the χ^2/dof for the full 91.25 set is considerably worse.

Here a comment is in order. The simple formulae (5) and (7), in both models, rely on some side assumptions (e.g. the special distributions for cluster charge fluctuations needed for the introduction of the equivalent global cluster) that are not expected to be exactly fulfilled. Therefore, those formulae are to be taken as a zero-order approximation and not as a faithful representation of the real process. Deviations from the introduced assumption entail corrections to the formulae (5) and (7) which are nevertheless very difficult to estimate. The theoretical error involved in these formulae becomes important when the accuracy of measurements is comparable and, in this case, a bad χ^2 is to be expected. This is probably the case at $\sqrt{s} = 91.25$ GeV, where the relative accuracy of measurements is of the order of few percent for many particles. In this case, the χ^2 fit is a useful tool to determine the best parameters of the "simplified" theory but should be used very carefully as a measure of the fit quality. As has been mentioned, in order to take into account the uncertainty on parameters implied in fits with $\chi^2/\text{dof} > 1$, parameter errors have been rescaled by $\sqrt{\chi^2/\text{dof}}$ if this is larger than 1, according to Particle Data Group procedure [40].

Table 5 Best fit parameters for the statistical hadronization model in e^+e^- collisions. The golden sample fit is marked with a $*$

$\sqrt{s}$	T [MeV]	VT^3	γ_S	χ^2/dof
14	172.1 ± 5.2	8.3 ± 1.0	0.772 ± 0.094	0.9/3
22	178.7 ± 3.7	8.70 ± 0.94	0.76 ± 0.10	0.7/3
29	164.0 ± 5.4	15.0 ± 2.4	0.683 ± 0.075	33/13
35	163.3 ± 3.2	15.0 ± 1.4	0.730 ± 0.045	8.2/7
43	169 ± 10	13.5 ± 3.2	0.741 ± 0.074	2.9/3
91	161.9 ± 4.1	25.8 ± 3.4	0.638 ± 0.039	215/27
91*	164.6 ± 3.0	23.3 ± 2.2	0.648 ± 0.026	39/12
133	167.1 ± 7.5	26.0 ± 4.6	0.671 ± 0.074	0.1/2
161	153.4 ± 6.5	37.2 ± 5.9	0.72 ± 0.12	0.03/1
183	161 ± 13	35 ± 11	0.446 ± 0.098	5.0/2
189	159 ± 12	36 ± 10	0.54 ± 0.11	7.5/2

For all the remaining energies we have also carried out the corresponding analyses; the results are listed in Tables 5 and 6 for the model parameters, while the comparison be-

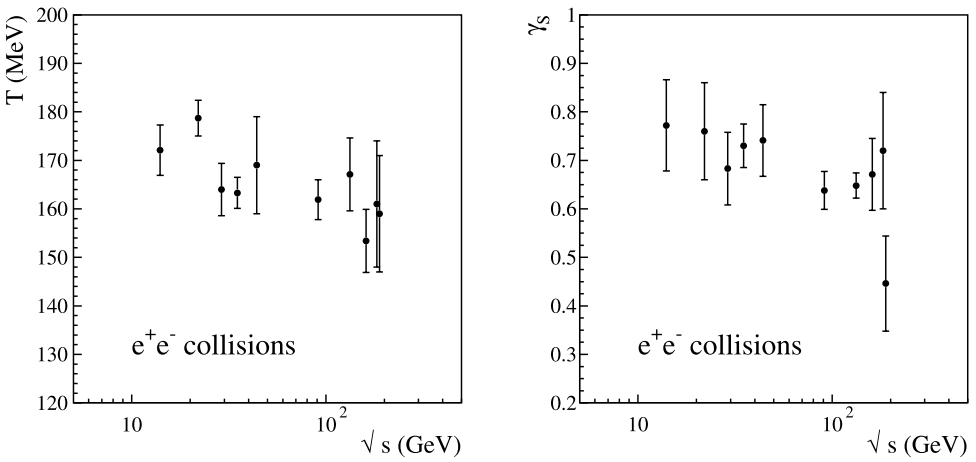

Fig. 5 Hadronization temperature T (*left*) and strangeness suppression factor γ_s (*right*) from conventional statistical fits to hadron abundances in e^+e^- annihilation, as function of the incident energy $\sqrt{s}$

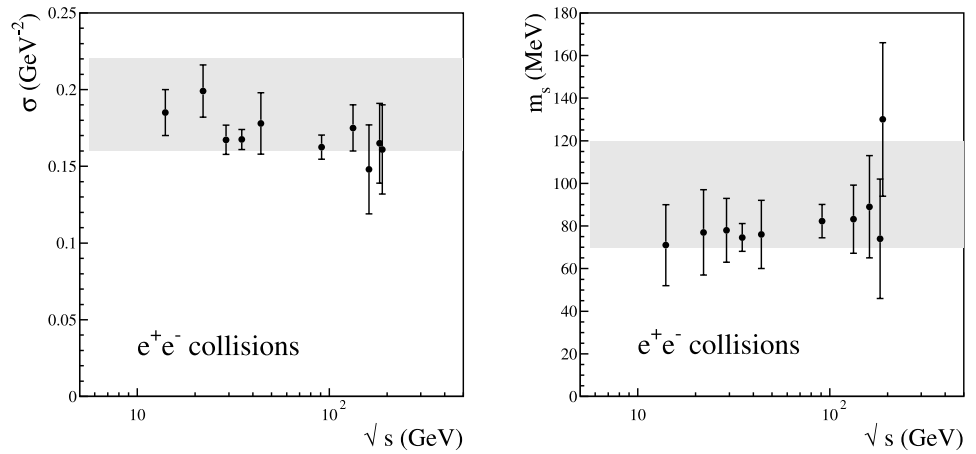

Fig. 6 String tension (*left*) and strange quark mass (*right*) from Hawking–Unruh fits to hadron abundances in e^+e^- annihilation, as function of the incident energy $\sqrt{s}$. The shaded bands give the overall average values as determined by other data

Table 6 Best fit parameters for the Hawking–Unruh model in e^+e^- collisions. The golden sample fit is marked with a $*$

$\sqrt{s}$	σ [GeV^2]	$V\sigma^{3/2}$	m_s [MeV]	χ^2/dof
14	0.185 ± 0.015	133 ± 24	71 ± 19	0.9/3
22	0.199 ± 0.017	140 ± 32	77 ± 20	0.7/3
29	0.1673 ± 0.0096	240 ± 36	78 ± 15	38/13
35	0.1675 ± 0.0065	237 ± 23	74.6 ± 6.5	8.8/7
43	0.178 ± 0.020	216 ± 48	76 ± 16	3.2/3
91	0.1625 ± 0.0078	406 ± 52	82.3 ± 7.8	217/27
91*	0.1683 ± 0.0042	368 ± 24	83.2 ± 4.0	23/12
133	0.175 ± 0.015	418 ± 69	89 ± 16	0.1/2
161	0.148 ± 0.029	590 ± 220	74 ± 24	0.03/1
183	0.165 ± 0.026	550 ± 160	130 ± 28	5.1/2
189	0.161 ± 0.029	560 ± 180	110 ± 36	7.7/2

tween measured and calculated multiplicities are shown in Tables 10 to 29 of the appendix.

The parameters T, γ_s and σ, m_s are shown in Figs. 5 and 6 respectively. It can be seen that they are remarkably constant throughout the examined energy range, from $\sqrt{s} = 14$ to 189 GeV.

Table 7 Hadronization temperatures for hadrons of different strangeness content, for $m_s = 0.083$ GeV and $\sigma = 0.169$ GeV^2

T [GeV]	
$T(00)$	0.164
$T(0s)$	0.156
$T(ss)$	0.148
$T(000)$	0.164
$T(00s)$	0.158
$T(0ss)$	0.153
$T(sss)$	0.148

We now recall that the quantities we treated as fit parameters in the Hawking–Unruh analyses, the string tension and the strange quark mass, have in fact been determined in various other contexts and by different methods; they are quite well known. The string tension σ is obtained in studies of heavy quarkonium spectroscopy as well as from Regge phenomenology. The canonical value [42] was 0.192 GeV^2; more recent calculations range from 0.16 GeV^2 [43, 44] to 0.22 GeV^2 [45–47], giving an estimate of $\sigma = 0.19 \pm 0.03$. The best average value of the strange quark mass is presently listed as [40] $m_s =$

Table 8 Abundances of charmed hadrons in $e^+e^- \to c\bar{c}$ annihilations and bottomed hadrons in $e^+e^- \to b\bar{b}$ annihilations at $\sqrt{s} = 91.25$ GeV, compared to the prediction of the statistical model

Particle		Experiment (E)	Model (M)	Residual	(M − E)/E [%]
D^0	[51]	0.559 ± 0.022	0.5406	−0.83	−3.2
D^+	[51]	0.238 ± 0.024	0.2235	−0.60	−6.1
D^{*+}	[51–53]	0.2377± 0.0098	0.2279	−1.00	−4.1
D^{*0}	[54]	0.218 ± 0.071	0.2311	0.18	6.0
D_1^0	[55, 56]	0.0173 ± 0.0039	0.01830	0.26	5.8
D_2^{*0}	[55, 56]	0.0484 ± 0.0080	0.02489	−2.94	−48.6
D_s	[51]	0.116 ± 0.036	0.1162	0.006	0.19
D_s^*	[51]	0.069 ± 0.026	0.0674	−0.06	−2.4
D_{s1}	[56, 57]	0.0106 ± 0.0025	0.00575	−1.94	−45.7
D_{s2}^*	[57]	0.0140 ± 0.0062	0.00778	−1.00	−44.5
Λ_c	[51]	0.079 ± 0.022	0.0966	0.80	22.2
$(B^0 + B^+)/2$	[58]	0.399 ± 0.011	0.3971	−0.18	−0.49
B_s	[58]	0.098 ± 0.012	0.1084	0.87	10.6
B^*/B(uds)	[59–62]	0.749 ± 0.040	0.6943	−1.37	−7.3
$B^{**} \times BR(B(^*)\pi)$	[63–65]	0.180 ± 0.025	0.1319	−1.92	−26.7
$(B_2^* + B_1) \times BR(B(^*)\pi)$	[64]	0.090 ± 0.018	0.0800	−0.57	−11.4
$B_{s2}^* \times BR(BK)$	[64]	0.0093 ± 0.0024	0.00631	−1.24	−32.1
b-baryon	[58]	0.103 ± 0.018	0.09751	−0.30	−5.3
Ξ_b^-	[58]	0.011 ± 0.006	0.00944	−0.26	−14.2

Table 9 Abundances of charmed hadrons in $e^+e^- \to c\bar{c}$ annihilations and bottomed hadrons in $e^+e^- \to b\bar{b}$ annihilations at $\sqrt{s} = 91.25$ GeV, compared to the prediction of the Hawking–Unruh radiation model

Particle		Experiment (E)	Model (M)	Residual	(M − E)/E [%]
D^0	[51]	0.559 ± 0.022	0.5635	0.20	0.81
D^+	[51]	0.238 ± 0.024	0.2332	−0.20	−2.0
D^{*+}	[51–53]	0.2377± 0.0098	0.2373	−0.04	−0.18
D^{*0}	[54]	0.218 ± 0.071	0.2407	0.32	10.4
D_1^0	[55, 56]	0.0173 ± 0.0039	0.01897	0.43	9.6
D_2^{*0}	[55, 56]	0.0484 ± 0.0080	0.02577	−2.82	−46.8
D_s	[51]	0.116 ± 0.036	0.08460	−0.87	−27.1
D_s^*	[51]	0.069 ± 0.026	0.04793	−0.81	−30.5
D_{s1}	[56, 57]	0.0106 ± 0.0025	0.00356	−2.82	−66.5
D_{s2}^*	[57]	0.0140 ± 0.0062	0.00479	−1.49	−66.1
Λ_c	[51]	0.079 ± 0.022	0.09922	0.92	25.6
$(B^0 + B^+)/2$	[58]	0.399 ± 0.011	0.4390	3.64	10.0
B_s	[58]	0.098 ± 0.012	0.0276	−5.87	−71.9
B^*/B(uds)	[59–62]	0.749 ± 0.040	0.6978	−1.28	−6.8
$B^{**} \times BR(B(^*)\pi)$	[63–65]	0.180 ± 0.025	0.1479	−1.28	−17.8
$(B_2^* + B_1) \times BR(B(^*)\pi)$	[64]	0.090 ± 0.018	0.0894	−0.04	−0.72
$B_{s2}^* \times BR(BK)$	[64]	0.0093 ± 0.0024	0.00136	−3.31	−85.3
b-baryon	[58]	0.103 ± 0.018	0.0944	−0.48	−8.4
Ξ_b^-	[58]	0.011 ± 0.006	0.00415	−1.14	−62.2

0.095 ± 0.025 GeV. In both cases we have good agreement with our fit values, as seen in Fig. 6. We may thus indeed conclude that the Hawking–Unruh approach provides a parameter-free description of thermal hadron abundances in e^+e^- annihilation. The suppression of hadrons containing strange quarks is fully accounted for in terms of slight temperature changes due to the heavier strange quark mass. It is thus natural that this affects also non-strange

hadrons dominantly made up of strange quarks, such as the ϕ.

To illustrate the effect, we list in Table 7 the different temperatures resulting from the different strange quark contents of the observed hadrons, using the fit parameters from the golden 91.25 data set. To check what such temperature differences may lead to, we compare the rate of direct ϕ production in the conventional to that of the Hawking–Unruh scenario. This direct rate is given by

$$\langle n\rangle_\phi = 3\frac{VTm^2}{2\pi^2}\mathrm{K}_2(m/T)\gamma_S^2 \tag{28}$$

in the conventional scenario; using the values (26) together with the production value listed in Table 5, we obtain $\langle n\rangle_\phi \simeq 0.078$. Note that $\gamma_s^2 \simeq 0.42$ reduces the equilibrium value by more than a factor of two. The Hawking–Unruh scheme has with $T(ss) = 0.148$ GeV a lower temperature for a meson containing a strange quark–antiquark pair than that governing light quark mesons. With

$$\langle n\rangle_\phi = 3\frac{VT(ss)m^2}{2\pi^2}\mathrm{K}_2\big(m/T(ss)\big) \tag{29}$$

and the corresponding production volume of Table 6, this leads to $\langle n\rangle_\phi \simeq 0.077$ and hence practically the same value, however, without invoking the parameter γ_s. We note that these results should not be compared directly to the ϕ production measured in e^+e^- annihilation, which contains (at 91.25 GeV) a further 30% due to feed-down contributions from charmed and bottomed hadron decay.

5.2 Heavy-flavored hadrons

As has been mentioned in the previous section, the calculation of heavy flavored-hadron yields in $e^+e^- \to c\bar{c}$ and $e^+e^- \to b\bar{b}$ events is necessary to determine the final light-flavored hadron multiplicities. The heavy-flavored hadron relative abundances in such events are determined according to formula (7). For the conventional formulation of the statistical model, one has the same temperature as for the light-flavored hadron species, while for the Hawking–Unruh radiation model, we do not have a definite prescription and we chose to use the same temperatures as for the light-flavored hadrons, which are dependent on the quark content.

Once the model parameters have been fit by using light-flavored hadronic multiplicities, they can be used to predict the relative yields of heavy-flavored species in $e^+e^- \to c\bar{c}$ and $e^+e^- \to b\bar{b}$ annihilations and compare them to measured ones. This is a powerful, parameter-free, independent test of the conventional statistical model and a necessary consistency check for the Hawking–Unruh radiation model. Also, comparing theoretical values to measured relative abundances of heavy-flavored hadrons

Table 10 Hadron multiplicities in e^+e^- collisions at 14 GeV, compared to the outcomes of the fit based on the statistical hadronization model with T and γ_S. The third and fourth columns show the differences between data and model in units of standard error and in percentages, respectively

		Experiment (E)	Model (M)	Residual	(M − E)/E (%)
π^0	[66]	4.69 ± 0.20	4.65	−0.18	−0.752
π^+	[67]	3.60 ± 0.30	3.79	0.62	5.18
K^+	[67]	0.600 ± 0.070	0.589	−0.15	−1.81
K_S^0	[67, 68]	0.563 ± 0.045	0.556	−0.15	−1.17
p	[67]	0.210 ± 0.030	0.199	−0.37	−5.36
Λ	[67]	0.065 ± 0.020	0.077	0.58	17.8

Table 11 Hadron multiplicities in e^+e^- collisions at 14 GeV, compared to the outcomes of the fit based on Hawking–Unruh radiation model. The third and fourth columns show the differences between data and model in units of standard error and in percentages, respectively

		Experiment (E)	Model (M)	Residual	(M − E)/E (%)
π^0	[66]	4.69 ± 0.20	4.66	−0.17	−0.712
π^+	[67]	3.60 ± 0.30	3.79	0.62	5.16
K^+	[67]	0.600 ± 0.070	0.589	−0.16	−1.85
K_S^0	[67, 68]	0.563 ± 0.045	0.556	−0.14	−1.14
p	[67]	0.210 ± 0.030	0.198	−0.39	−5.52
Λ	[67]	0.065 ± 0.020	0.077	0.58	17.8

Table 12 Hadron multiplicities in e^+e^- collisions at 22 GeV, compared to the outcomes of the fit based on the statistical hadronization model with T and γ_S. The third and fourth columns show the differences between data and model in units of standard error and in percentages, respectively

		Experiment (E)	Model (M)	Residual	(M − E)/E (%)
π^0	[66]	5.50 ± 0.40	5.49	−0.033	−0.238
π^+	[67]	4.40 ± 0.50	4.54	0.28	3.16
K^+	[67]	0.75 ± 0.10	0.69	−0.65	−8.64
K_S^0	[68, 69]	0.638 ± 0.057	0.651	0.22	1.96
p	[67]	0.310 ± 0.030	0.305	−0.16	−1.51
Λ	[67]	0.110 ± 0.025	0.117	0.29	6.70

Table 13 Hadron multiplicities in e^+e^- collisions at 22 GeV, compared to the outcomes of the fit based on Hawking–Unruh radiation model. The third and fourth columns show the differences between data and model in units of standard error and in percentages, respectively

		Experiment (E)	Model (M)	Residual	(M − E)/E (%)
π^0	[66]	5.50 ± 0.40	5.49	−0.020	−0.148
π^+	[67]	4.40 ± 0.50	4.54	0.28	3.18
K^+	[67]	0.75 ± 0.10	0.68	−0.65	−8.71
K_S^0	[68, 69]	0.638 ± 0.057	0.651	0.22	1.94
p	[67]	0.310 ± 0.030	0.305	−0.17	−1.65
Λ	[67]	0.110 ± 0.025	0.118	0.31	7.02

Table 14 Hadron multiplicities in e^+e^- collisions at 29 GeV, compared to the outcomes of the fit based on the statistical hadronization model with T and γ_S. The third and fourth columns show the differences between data and model in units of standard error and in percentages, respectively

		Experiment (E)	Model (M)	Residual	(M − E)/E (%)
π^0	[70]	5.30 ± 0.70	6.48	1.7	22.2
π^+	[71]	5.35 ± 0.25	5.42	0.26	1.23
K^+	[71]	0.700 ± 0.050	0.747	0.93	6.66
K^0_S	[72–74]	0.691 ± 0.029	0.712	0.73	3.05
η	[75, 76]	0.584 ± 0.075	0.654	0.92	11.8
ρ^0	[77]	0.900 ± 0.050	0.745	−3.1	−17.2
K^{*+}	[78]	0.310 ± 0.030	0.237	−2.4	−23.7
K^{*0}	[73, 77]	0.281 ± 0.022	0.232	−2.2	−17.3
p	[71]	0.300 ± 0.050	0.300	0.0038	0.0627
η'	[76]	0.26 ± 0.10	0.07	−1.8	−71.6
ϕ	[79]	0.084 ± 0.022	0.092	0.35	9.15
Λ	[80–82]	0.0983 ± 0.0060	0.1016	0.56	3.43
Ξ^-	[83, 84]	0.0083 ± 0.0020	0.0070	−0.64	−15.4
Σ^{*+}	[84]	0.0083 ± 0.0024	0.0111	1.2	34.2
K^{*+}_2	[78]	0.045 ± 0.022	0.016	−1.3	−64.4
Ω	[85]	0.0070 ± 0.0036	0.0005	−1.8	−93.4

Table 15 Hadron multiplicities in e^+e^- collisions at 29 GeV, compared to the outcomes of the fit based on Hawking–Unruh radiation model. The third and fourth columns show the differences between data and model in units of standard error and in percentages, respectively

		Experiment (E)	Model (M)	Residual	(M − E)/E (%)
π^0	[70]	5.30 ± 0.70	6.37	1.5	20.2
π^+	[71]	5.35 ± 0.25	5.31	−0.15	−0.715
K^+	[71]	0.700 ± 0.050	0.760	1.2	8.55
K^0_S	[72–74]	0.691 ± 0.029	0.725	1.2	4.96
η	[75, 76]	0.584 ± 0.075	0.643	0.78	10.0
ρ^0	[77]	0.900 ± 0.050	0.727	−3.5	−19.2
K^{*+}	[78]	0.310 ± 0.030	0.231	−2.6	−25.6
K^{*0}	[73, 77]	0.281 ± 0.022	0.227	−2.4	−19.3
p	[71]	0.300 ± 0.050	0.292	−0.17	−2.82
η'	[76]	0.26 ± 0.10	0.07	−1.9	−75.0
ϕ	[79]	0.084 ± 0.022	0.084	−0.022	−0.593
Λ	[80–82]	0.0983 ± 0.0060	0.1024	0.69	4.24
Ξ^-	[83, 84]	0.0083 ± 0.0020	0.0068	−0.72	−17.5
Σ^{*+}	[84]	0.0083 ± 0.0024	0.0111	1.2	34.8
K^{*+}_2	[78]	0.045 ± 0.022	0.014	−1.4	−69.9
Ω	[85]	0.0070 ± 0.0036	0.0004	−1.8	−94.6

in specific annihilation channels (e.g. charmed hadrons in $e^+e^- \to c\bar{c}$), we achieve a more effective test, because, e.g., the contribution of weak $b \to c$ decays is excluded.

The relative yields of several heavy-flavored hadronic species have been measured in e^+e^- collisions at 91.25 GeV by the four LEP experiments. We show a comparison between model and weighted averaged experimental values in Tables 8 and 9.

For the statistical model (Table 8), the theoretical values have been estimated by using the parameters in (26). The agreement between model and experiment is strikingly good, with few peculiar deviations in the heavier states. In all those cases we observe an underestimation of measured values, which may partly be explained by the absence, in our input spectrum, of unknown heavier heavy-flavored resonances feeding these states. It is quite remarkable that the model is able to reproduce the largely different V/P ratios in the charm (D^*/D) and bottomed (B^*/B) sector—a long-standing issue in string models—without any additional parameter. This result confirms previous early findings [1, 48].

For the Hawking–Unruh radiation model (Table 9), the agreement between the theoretical multiplicities calcu-

Table 16 Hadron multiplicities in e^+e^- collisions at 35 GeV, compared to the outcomes of the fit based on the statistical hadronization model with T and γ_S. The third and fourth columns show the differences between data and model in units of standard error and in percentages, respectively

		Experiment (E)	Model (M)	Residual	(M − E)/E (%)
π^0	[86–88]	6.31 ± 0.35	6.48	0.49	2.73
π^+	[89]	5.45 ± 0.25	5.42	−0.14	−0.621
K^+	[89]	0.88 ± 0.10	0.78	−0.98	−11.2
K^0_S	[68, 69, 90]	0.740 ± 0.017	0.746	0.33	0.759
η	[87, 88]	0.636 ± 0.080	0.661	0.32	4.06
ρ^0	[67, 91]	0.756 ± 0.077	0.739	−0.23	−2.30
K^{*+}	[69, 90, 91]	0.361 ± 0.046	0.248	−2.4	−31.2
p	[89, 92]	0.302 ± 0.033	0.300	−0.078	−0.838
Λ	[90, 93]	0.108 ± 0.010	0.108	−0.042	−0.391
Ξ^-	[93]	0.0060 ± 0.0021	0.0079	0.90	31.5

Table 17 Hadron multiplicities in e^+e^- collisions at 35 GeV, compared to the outcomes of the fit based on Hawking–Unruh radiation model. The third and fourth columns show the differences between data and model in units of standard error and in percentages, respectively

		Experiment (E)	Model (M)	Residual	(M − E)/E (%)
π^0	[86–88]	6.31 ± 0.35	6.46	0.41	2.31
π^+	[89]	5.45 ± 0.25	5.39	−0.25	−1.13
K^+	[89]	0.88 ± 0.10	0.78	−0.97	−11.0
K^0_S	[68, 69, 90]	0.740 ± 0.017	0.748	0.47	1.08
η	[87, 88]	0.636 ± 0.080	0.657	0.26	3.33
ρ^0	[67, 91]	0.756 ± 0.077	0.735	−0.28	−2.82
K^{*+}	[69, 90, 91]	0.361 ± 0.046	0.239	−2.6	−33.6
p	[89, 92]	0.302 ± 0.033	0.301	−0.042	−0.450
Λ	[90, 93]	0.108 ± 0.010	0.108	0.028	0.261
Ξ^-	[93]	0.0060 ± 0.0021	0.0075	0.70	24.4

Table 18 Hadron multiplicities in e^+e^- collisions at 43 GeV, compared to the outcomes of the fit based on the statistical hadronization model with T and γ_S. The third and fourth columns show the differences between data and model in units of standard error and in percentages, respectively

		Experiment (E)	Model (M)	Residual	(M − E)/E (%)
π^0	[87, 89]	6.66 ± 0.65	6.63	−0.055	−0.541
π^+	[89]	5.55 ± 0.25	5.55	−0.0021	−0.00955
K^+	[94]	0.96 ± 0.15	0.81	−1.0	−15.9
K^0_S	[69]	0.760 ± 0.035	0.775	0.43	2.01
K^{*+}	[69]	0.385 ± 0.094	0.264	−1.3	−31.3
Λ	[93]	0.128 ± 0.024	0.131	0.12	2.23

Table 19 Hadron multiplicities in e^+e^- collisions at 43 GeV, compared to the outcomes of the fit based on Hawking–Unruh radiation model. The third and fourth columns show the differences between data and model in units of standard error and in percentages, respectively

		Experiment (E)	Model (M)	Residual	(M − E)/E (%)
π^0	[87, 89]	6.66 ± 0.65	6.62	−0.065	−0.639
π^+	[89]	5.55 ± 0.25	5.54	−0.042	−0.188
K^+	[94]	0.96 ± 0.15	0.81	−1.0	−15.8
K^0_S	[69]	0.760 ± 0.035	0.777	0.47	2.18
K^{*+}	[69]	0.385 ± 0.094	0.255	−1.4	−33.6
Λ	[93]	0.128 ± 0.024	0.131	0.13	2.52

lated with the parameters in (27) and experiment is generally good, although not as good as for the conventional scheme. In fact, there are some specific discrepancies, especially in the beauty sector. In particular, we underestimate the relative yield of B_s mesons, which is an effect of the lower temperature for open strange particles combined with the high mass of these particles, compared to light-flavored species. In general, the way heavy-flavored hadrons are to be calculated in this model is still an open issue.

6 Conclusions

We have shown that in accord with previous studies [1–3], the thermal hadron abundances observed in e^+e^- collisions over a wide range of energies can indeed be accounted for in an ideal resonance gas scenario, based on a universal temperature $T \simeq 165$ MeV and a strangeness suppression factor $\gamma_s \simeq 0.7$. The latter is the ad hoc price paid in order to account for the deviation from full chemical equilibrium observed in the data. Remarkably, also the relative abundances of heavy-flavored species

Table 20 Hadron multiplicities in e^+e^- collisions at 91 GeV, compared to the outcomes of the fit based on the statistical hadronization model with T and γ_S. The third and fourth columns show the differences between data and model in units of standard error and in percentages, respectively

		Experiment (E)	Model (M)	Residual	(M − E)/E (%)
π^0	[95–98]	9.61 ± 0.29	10.20	2.0	6.18
π^+	[99–102]	8.50 ± 0.10	8.76	2.6	3.13
K^+	[99–102]	1.127 ± 0.026	1.091	−1.4	−3.20
K_S^0	[95, 98, 102, 103, 105]	1.0376 ± 0.0096	1.0507	1.4	1.26
η	[95, 98, 106]	1.059 ± 0.086	1.041	−0.21	−1.70
ρ^0	[107, 108]	1.40 ± 0.13	1.19	−1.6	−15.0
ρ^+	[109]	1.20 ± 0.22	1.14	−0.26	−4.66
ω	[106, 109, 110]	1.024 ± 0.059	1.014	−0.17	−0.997
K^{*+}	[103, 104, 111]	0.357 ± 0.022	0.353	−0.16	−1.02
K^{*0}	[102, 104, 112, 113]	0.370 ± 0.013	0.346	−1.9	−6.33
p	[99–102]	0.519 ± 0.018	0.564	2.5	8.76
η'	[109, 110]	0.166 ± 0.047	0.106	−1.3	−36.1
f_0	[107, 108, 114]	0.1555 ± 0.0085	0.0779	−9.1	−49.9
a_0^+	[109]	0.135 ± 0.054	0.084	−0.95	−37.8
ϕ	[102, 104, 113, 114]	0.0977 ± 0.0058	0.1150	3.0	17.7
Λ	[95, 102, 105, 115, 116]	0.1943 ± 0.0038	0.1779	−4.3	−8.42
Σ^+	[117–119]	0.0535 ± 0.0052	0.0415	−2.3	−22.4
Σ^0	[104, 118–120]	0.0389 ± 0.0041	0.0421	0.77	8.11
Σ^-	[118, 121]	0.0410 ± 0.0037	0.0378	−0.85	−7.65
Δ^{++}	[122, 123]	0.044 ± 0.017	0.090	2.7	105.
f_2	[107, 108, 114]	0.188 ± 0.020	0.122	−3.4	−35.1
f_1	[124]	0.165 ± 0.051	0.064	−2.0	−61.5
Ξ^-	[104, 116, 117]	0.01319 ± 0.00050	0.01187	−2.6	−10.0
Σ^{*+}	[104, 116, 117]	0.0118 ± 0.0011	0.0201	7.5	70.3
f_1'	[124]	0.056 ± 0.012	0.010	−3.9	−82.6
K_{20}^*	[107]	0.036 ± 0.012	0.026	−0.91	−29.2
$\Lambda(1520)$	[116, 121]	0.0112 ± 0.0014	0.0109	−0.22	−2.73
f_2'	[107]	0.0120 ± 0.0058	0.0100	−0.34	−16.6
Ξ^{*0}	[104, 116, 117]	0.00289 ± 0.00050	0.00417	2.6	44.4
Ω	[104, 116, 120]	0.00062 ± 0.00010	0.00081	1.9	31.0

are in very good agreement with the statistical-thermal *ansatz*.

The Hawking–Unruh scenario, on the other hand, provides an intrinsic deviation from full equilibrium through the dependence of the radiation temperature on the mass of the emitted quark. Given the value of this mass and the string tension specifying the field strength at the confinement horizon, we then have a parameter-free prediction of the relative hadron abundances. We have seen here that these predictions agree well with the data at all energies, with the caveat that the relative multiplicities of heavy-flavored hadron species are not completely understood in this picture and are in slightly worse agreement with respect to the conventional statistical model. In a subsequent paper, we shall extend the Hawking–Unruh description to high energy heavy ion collisions, where it becomes significantly modified.

In closing, we comment on the degree of agreement between experiment and theory in our description. Hawking–Unruh radiation is thermal in leading order [49], with higher-order interaction terms. Similarly, one expects corrections to the simplest statistical hadronization model formulae, see discussion in Sect. 4. When accuracy of measurements is good enough, such higher-order effects must be taken into account and the fit quality to the simplest formulae unavoidably degrades. It is an interesting question to see if nuclear collisions, with a higher degree of averaging, lead to smaller deviations with measurements of the same accuracy.

Appendix

In the following Tables 10–29, the experimental data and the statistical hadronization model predictions for var-

Table 21 Hadron multiplicities in e^+e^- collisions at 91 GeV, compared to the outcomes of the fit based on the Hawking–Unruh radiation model. The third and fourth columns show the differences between data and model in units of standard error and in percentages, respectively

		Experiment (E)	Model (M)	Residual	(M − E)/E (%)
π^0	[95–98]	9.61 ± 0.29	10.01	1.4	4.18
π^+	[99–102]	8.50 ± 0.10	8.57	0.77	0.918
K^+	[99–102]	1.127 ± 0.026	1.131	0.16	0.373
K_S^0	[95, 98, 102, 103, 105]	1.0376 ± 0.0096	1.0901	5.5	5.05
η	[95, 98, 106]	1.059 ± 0.086	1.026	−0.38	−3.12
ρ^0	[107, 108]	1.40 ± 0.13	1.15	−1.9	−17.4
ρ^+	[109]	1.20 ± 0.22	1.11	−0.42	−7.53
ω	[106, 109, 110]	1.024 ± 0.059	0.982	−0.71	−4.08
K^{*+}	[103, 104, 111]	0.357 ± 0.022	0.345	−0.54	−3.36
K^{*0}	[102, 104, 112, 113]	0.370 ± 0.013	0.338	−2.5	−8.62
p	[99–102]	0.519 ± 0.018	0.548	1.6	5.67
η'	[109, 110]	0.166 ± 0.047	0.093	−1.6	−43.8
f_0	[107, 108, 114]	0.1555 ± 0.0085	0.0751	−9.5	−51.7
a_0^+	[109]	0.135 ± 0.054	0.081	−1.0	−40.0
ϕ	[102, 104, 113, 114]	0.0977 ± 0.0058	0.1048	1.2	7.19
Λ	[95, 102, 105, 115, 116]	0.1943 ± 0.0038	0.1826	−3.1	−6.04
Σ^+	[117–119]	0.0535 ± 0.0052	0.0424	−2.1	−20.7
Σ^0	[104, 118–120]	0.0389 ± 0.0041	0.0430	1.00	10.5
Σ^-	[118, 121]	0.0410 ± 0.0037	0.0388	−0.59	−5.31
Δ^{++}	[122, 123]	0.044 ± 0.017	0.086	2.5	95.0
f_2	[107, 108, 114]	0.188 ± 0.020	0.115	−3.7	−38.9
f_1	[124]	0.165 ± 0.051	0.061	−2.0	−63.2
Ξ^-	[104, 116, 117]	0.01319 ± 0.00050	0.01204	−2.3	−8.72
Σ^{*+}	[104, 116, 117]	0.0118 ± 0.0011	0.0204	7.8	72.8
f_1'	[124]	0.056 ± 0.012	0.007	−4.1	−87.3
K_{20}^*	[107]	0.036 ± 0.012	0.021	−1.3	−41.7
$\Lambda(1520)$	[116, 121]	0.0112 ± 0.0014	0.0106	−0.45	−5.55
f_2'	[107]	0.0120 ± 0.0058	0.0068	−0.89	−43.1
Ξ^{*0}	[104, 116, 117]	0.00289 ± 0.00050	0.00423	2.7	46.4
Ω	[104, 116, 120]	0.00062 ± 0.00010	0.00071	0.85	13.8

Table 22 Hadron multiplicities in e^+e^- collisions at 133 GeV, compared to the outcomes of the fit based on the statistical hadronization model with T and γ_S. The third and fourth columns show the differences between data and model in units of standard error and in percentages, respectively

		Experiment (E)	Model (M)	Residual	(M − E)/E (%)
π^+	[125]	9.92 ± 0.26	9.94	0.063	0.167
K^+	[125]	1.30 ± 0.15	1.29	−0.064	−0.714
K_S^0	[125]	1.25 ± 0.12	1.25	−0.070	−0.663
p	[125]	0.78 ± 0.13	0.75	−0.19	−3.26
Λ	[125]	0.250 ± 0.038	0.256	0.15	2.27

Table 23 Hadron multiplicities in e^+e^- collisions at 133 GeV, compared to the outcomes of the fit based on the Hawking–Unruh radiation model. The third and fourth columns show the differences between data and model in units of standard error and in percentages, respectively

		Experiment (E)	Model (M)	Residual	(M − E)/E (%)
π^+	[125]	9.92 ± 0.26	9.94	0.059	0.157
K^+	[125]	1.30 ± 0.15	1.29	−0.060	−0.669
K_S^0	[125]	1.25 ± 0.12	1.25	−0.056	−0.533
p	[125]	0.78 ± 0.13	0.76	−0.17	−2.92
Λ	[125]	0.250 ± 0.038	0.255	0.13	1.92

ious hadron multiplicities are compared. The first column shows the experimental value while in the second column, the statistical hadronization model prediction is quoted. In the fourth column one can find the relative deviation of the model from the experiment in percentage, while the third column shows the residuals defined as

$$\text{Residual}_i = \frac{N_i^{\text{th}} - N_i^{\text{ex}}}{\sigma_i} \tag{30}$$

Table 24 Hadron multiplicities in e^+e^- collisions at 161 GeV, compared to the outcomes of the fit based on the statistical hadronization model with T and γ_S. The third and fourth columns show the differences between data and model in units of standard error and in percentages, respectively

		Experiment (E)	Model (M)	Residual	(M − E)/E (%)
π^+	[125]	10.38 ± 0.38	10.37	−0.00096	−0.00355
K^+	[125]	1.44 ± 0.30	1.39	−0.15	−3.12
K^0_S	[125]	1.32 ± 0.18	1.34	0.094	1.31
p	[125]	0.60 ± 0.24	0.60	−0.0010	−0.0414

Table 25 Hadron multiplicities in e^+e^- collisions at 161 GeV, compared to the outcomes of the fit based on Hawking–Unruh radiation model. The third and fourth columns show the differences between data and model in units of standard error and in percentages, respectively

		Experiment (E)	Model (M)	Residual	(M − E)/E (%)
π^+	[125]	10.38 ± 0.38	10.37	−0.0012	−0.00431
K^+	[125]	1.44 ± 0.30	1.39	−0.15	−3.18
K^0_S	[125]	1.32 ± 0.18	1.34	0.097	1.34
p	[125]	0.60 ± 0.24	0.60	−0.0011	−0.0436

Table 26 Hadron multiplicities in e^+e^- collisions at 183 GeV, compared to the outcomes of the fit based on the statistical hadronization model with T and γ_S. The third and fourth columns show the differences between data and model in units of standard error and in percentages, respectively

		Experiment (E)	Model (M)	Residual	(M − E)/E (%)
π^+	[125]	10.89 ± 0.29	10.87	−0.081	−0.216
K^+	[125]	1.42 ± 0.20	1.03	−2.0	−27.2
K^0_S	[125]	0.905 ± 0.086	0.995	1.0	9.97
p	[125]	0.66 ± 0.19	0.71	0.25	7.13
Λ	[125]	0.165 ± 0.025	0.161	−0.15	−2.35

Table 27 Hadron multiplicities in e^+e^- collisions at 183 GeV, compared to the outcomes of the fit based on Hawking–Unruh radiation model. The third and fourth columns show the differences between data and model in units of standard error and in percentages, respectively

		Experiment (E)	Model (M)	Residual	(M − E)/E (%)
π^+	[125]	10.89 ± 0.29	10.86	−0.12	−0.326
K^+	[125]	1.42 ± 0.20	1.03	−1.9	−27.0
K^0_S	[125]	0.905 ± 0.086	0.999	1.1	10.4
p	[125]	0.66 ± 0.19	0.73	0.36	10.5
Λ	[125]	0.165 ± 0.025	0.160	−0.20	−3.08

in which $N_i^{\rm th}$ and $N_i^{\rm ex}$ are the theoretical and experimental multiplicities and σ_i is the (experimental) standard error of a particle species i. For each of the energies, we show two different tables, one after the other, so that always the first table shows the conventional statistical hadronization model

Table 28 Hadron multiplicities in e^+e^- collisions at 189 GeV, compared to the outcomes of the fit based on the statistical hadronization model with T and γ_S. The third and fourth columns show the differences between data and model in units of standard error and in percentages, respectively

		Experiment (E)	Model (M)	Residual	(M − E)/E (%)
π^+	[125]	11.10 ± 0.26	11.06	−0.15	−0.344
K^+	[125]	1.57 ± 0.16	1.21	−2.3	−23.2
K^0_S	[125]	1.060 ± 0.078	1.169	1.4	10.3
p	[125]	0.59 ± 0.22	0.72	0.54	20.3
Λ	[125]	0.200 ± 0.021	0.196	−0.20	−2.16

Table 29 Hadron multiplicities in e^+e^- collisions at 189 GeV, compared to the outcomes of the fit based on Hawking–Unruh radiation model. The third and fourth columns show the differences between data and model in units of standard error and in percentages, respectively

		Experiment (E)	Model (M)	Residual	(M − E)/E (%)
π^+	[125]	11.10 ± 0.26	11.05	−0.18	−0.422
K^+	[125]	1.57 ± 0.16	1.21	−2.3	−23.2
K^0_S	[125]	1.060 ± 0.078	1.171	1.4	10.5
p	[125]	0.59 ± 0.22	0.74	0.64	23.7
Λ	[125]	0.200 ± 0.021	0.195	−0.22	−2.31

fit results, while the following one shows the same information in the Hawking–Unruh approach.

Note added in proof

After completion of this work, another analysis of hadron production in e^+e^- annihilation has appeared, reaching very different conclusions [50]. However, in contrast to our work, it is assumed in that analysis that the conservation of charm and bottom can be neglected. In e^+e^- annihilation, more than 40% of all events contain a primary charm or bottom quark–antiquark pair (see our Table 2), hence two heavy-flavored hadrons. Neglecting the corresponding conservation conditions and the decay contributions of these heavy-flavored hadrons into light-flavored hadrons necessarily produces serious disagreement with the data, especially for strange particles.

References

1. F. Becattini, Z. Phys. C **69**, 485 (1996)
2. F. Becattini, in *Universality Features in Multihadron Production and the Leading Effect* (World Scientific, Singapore, 1998), pp. 74–104. arXiv:hep-ph/9701275
3. F. Becattini, G. Passaleva, Eur. Phys. J. **C23**, 551 (2002)
4. F. Becattini, U. Heinz, Z. Phys. C **76**, 268 (1997)
5. J. Cleymans et al., Phys. Lett. B **242**, 111 (1990)

6. J. Cleymans, H. Satz, Z. Phys. C **57**, 135 (1993)
7. K. Redlich et al., Nucl. Phys. A **566**, 391 (1994)
8. P. Braun-Munzinger et al., Phys. Lett. B **344**, 43 (1995)
9. F. Becattini, M. Gazdzicki, J. Sollfrank, Eur. Phys. J. **C5**, 143 (1998)
10. F. Becattini et al., Phys. Rev. C **64**, 024901 (2001)
11. P. Braun-Munzinger, K. Redlich, J. Stachel, in *Quark-Gluon Plasma 3*, ed. by R.C. Hwa, X.-N. Wang (World Scientific, Singapore, 2003)
12. F. Becattini, Nucl. Phys. A **702**, 336 (2001)
13. J. Letessier, J. Rafelski, A. Tounsi, Phys. Rev. C **64**, 406 (1994)
14. F. Becattini, J. Manninen, M. Gazdzicki, Phys. Rev. C **73**, 044905 (2006)
15. P. Braun-Munzinger, D. Magestro, K. Redlich, J. Stachel, Phys. Lett. B **518**, 41 (2001)
16. U. Heinz, Nucl. Phys. A **661**, 140 (1999)
17. R. Stock, Phys. Lett. B **456**, 277 (1999)
18. A. Bialas, Phys. Lett. B **466**, 301 (1999)
19. H. Satz, Nucl. Phys. Proc. Suppl. **94**, 204 (2001)
20. J. Hormuzdiar, S.D.H. Hsu, G. Mahlon, Int. J. Mod. Phys. E **12**, 649 (2003)
21. V. Koch, Nucl. Phys. A **715**, 108 (2003)
22. L. McLerran, arXiv:hep-ph/0311028
23. Y. Dokshitzer, Acta Phys. Polon. B **36**, 361 (2005)
24. F. Becattini, J. Phys. Conf. Ser. **5**, 175 (2005)
25. P. Castorina, D. Kharzeev, H. Satz, Eur. Phys. J. C **52**, 187 (2007)
26. S.W. Hawking, Commun. Math. Phys. **43**, 199 (1975)
27. W.G. Unruh, Phys. Rev. D **14**, 870 (1976)
28. J. Schwinger, Phys. Rev. **82**, 664 (1951)
29. R. Brout, R. Parentani, Ph. Spindel, Nucl. Phys. B **353**, 209 (1991)
30. P. Parentani, S. Massar, Phys. Rev. D **55**, 3603 (1997)
31. K. Srinivasan, T. Padmanabhan, Phys. Rev. D **60**, 024007 (1999)
32. D. Kharzeev, K. Tuchin, Nucl. Phys. A **753**, 316 (2005)
33. S.P. Kim, arXiv:0709.4313 [hep-th] (2007)
34. F. Becattini, J. Phys. Conf. Ser. **5**, 175 (2005)
35. F. Becattini, L. Ferroni, Eur. Phys. J. C **35**, 243 (2004)
36. F. Becattini, L. Ferroni, Eur. Phys. J. C **38**, 225 (2004)
37. A. Keranen, F. Becattini, Phys. Rev. C **65**, 044901 (2002); Erratum: Phys. Rev. C **68** (2003) 059901
38. J.D. Bjorken, in *Lecture Notes in Physics* vol. 56 (Springer, Berlin, 1979), p. 93.
39. A. Casher, H. Neuberger, S. Nussinov, Phys. Rev. D **20**, 179 (1979)
40. W.-M. Yao et al., J. Phys. G **33**, 1 (2006)
41. T. Sjostrand et al., Comput. Phys. Commun. **135**, 238 (2001)
42. S. Jacobs, M.G. Olsson, C. Suchyta, Phys. Rev. D **33**, 3338 (1986)
43. F.J. Yndurain, *Theory of Quark and Gluon Interactions* (Springer, Berlin, 1999)
44. N. Brambilla et al., CERN Yellow Report CERN-2005-005
45. MILC Collaboration, C. Aubin et al., Phys. Rev. D **70**, 094505 (2004)
46. A. Gray et al., Phys. Rev. D **72**, 0894507 (2005)
47. M. Cheng et al., arXiv:hep-lat/0608013
48. F. Becattini, J. Phys. G **23**, 1933 (1997)
49. M.K. Parikh, F. Wilczek, Phys. Rev. Lett. **85**, 5042 (2000)
50. A. Andronic, F. Beutler, P. Braun-Munzinger, K. Redlich, J. Stachel, arXiv:0804.4132
51. ALEPH Collaboration, R. Barate et al., Eur. Phys. J. C **16**, 597 (2000)
52. OPAL Collaboration, K. Ackerstaff et al., Eur. Phys. J. C **1**, 439 (1998)
53. DELPHI Collaboration, P. Abreu et al., Eur. Phys. J. C **12**, 209 (2000)
54. OPAL Collaboration, K. Ackerstaff et al., Eur. Phys. J. C **5**, 1 (1998)
55. The ALEPH Collaboration, preprint ALEPH 98-047 CONF 98-021 (1998)
56. OPAL Collaboration, K. Ackerstaff et al., Z. Phys. C **76**, 425 (1997)
57. ALEPH Collaboration, A. Heister et al., Phys. Lett. B **526**, 34 (2002)
58. The ALEPH, DELPHI, L3, OPAL and CDF Collaborations, arXiv:hep-ex/0112028
59. OPAL Collaboration, K. Ackerstaff et al., Z. Phys. C **74**, 413 (1997)
60. ALEPH Collaboration, D. Buskulic et al., Z. Phys. C **69**, 393 (1996)
61. DELPHI Collaboration, P. Abreu et al., Z. Phys. C **68**, 353 (1995)
62. L3 Collaboration, M. Acciarri et al., Phys. Lett. B **345**, 589 (1995)
63. ALEPH Collaboration, R. Barate et al., Phys. Lett. B **425**, 215 (1998)
64. DELPHI Collaboration, Z. Albrecht et al., preprint DELPHI-2004-025 CONF 700 (2004), presented at ICHEP 2004
65. OPAL Collaboration, R. Akers et al., Z. Phys. C **66**, 19 (1995)
66. JADE Collaboration, W. Bartel et al., Z. Phys. C **28**, 343 (1985)
67. TASSO Collaboration, M. Althoff et al., Z. Phys. C **27**, 27 (1985)
68. JADE Collaboration, W. Bartel et al., Z. Phys. C **20**, 187 (1983)
69. TASSO Collaboration, W. Braunschweig et al., Z. Phys. C **47**, 167 (1990)
70. TPC/Two Gamma Collaboration, H. Aihara et al., Z. Phys. C **27**, 187 (1985)
71. TPC/Two Gamma Collaboration, H. Aihara et al., Phys. Lett. B **184**, 299 (1987)
72. H. Schellman et al., Phys. Rev. D **31**, 3013 (1985)
73. TPC/Two Gamma Collaboration, H. Aihara et al., Phys. Rev. Lett. **53**, 2378 (1984)
74. HRS Collaboration, S. Abachi et al., Phys. Rev. D **41**, 2045 (1990)
75. HRS Collaboration, S. Abachi et al., Phys. Lett. B **205**, 111 (1988)
76. G. Wormser et al., Phys. Rev. Lett. **61**, 1057 (1988)
77. S. Abachi et al., Phys. Rev. D **40**, 706 (1989)
78. S. Abachi et al., Phys. Lett. B **199**, 151 (1987)
79. TPC/Two Gamma Collaboration, H. Aihara et al., Phys. Rev. Lett. **52**, 2201 (1984)
80. TPC/Two Gamma Collaboration, H. Aihara et al., Phys. Rev. Lett. **54**, 274 (1985)
81. C. de la Vaissiere et al., Phys. Rev. Lett. **54**, 2071 (1985). [Erratum-ibid. **55** (1985) 263]
82. HRS Collaboration, T.L. Geld et al., Phys. Rev. D **45**, 3949 (1992)
83. S. Klein et al., Phys. Rev. Lett. **58**, 644 (1987)
84. S. Abachi et al., Phys. Rev. Lett. **58**, 2627 (1987); Erratum: Phys. Rev. Lett. **59** (1987) 2388
85. S. Klein et al., Phys. Rev. Lett. **59**, 2412 (1987)
86. TASSO Collaboration, W. Braunschweig et al., Z. Phys. C **33**, 13 (1986)
87. JADE Collaboration, D. Pitzl et al., Z. Phys. C **46**, 1 (1990); Erratum: Z. Phyz. C **47** (1990) 676]
88. CELLO Collaboration, H.J. Behrend et al., Z. Phys. C **47**, 1 (1990)
89. TASSO Collaboration, W. Braunschweig et al., Z. Phys. C **42**, 189 (1989)
90. CELLO Collaboration, H.J. Behrend et al., Z. Phys. C **46**, 397 (1990)
91. JADE Collaboration, W. Bartel et al., Phys. Lett. B **145**, 441 (1984)
92. JADE Collaboration, W. Bartel et al., Phys. Lett. B **104**, 325 (1981)

93. TASSO Collaboration, W. Braunschweig et al., Z. Phys. C **45**, 209 (1989)
94. TASSO Collaboration, W. Braunschweig et al., Z. Phys. C **45**, 193 (1989)
95. L3 Collaboration, M. Acciarri et al., Phys. Lett. B **328**, 223 (1994)
96. DELPHI Collaboration, W. Adam et al., Z. Phys. C **69**, 561 (1996)
97. ALEPH Collaboration, R. Barate et al., Z. Phys. C **74**, 451 (1997)
98. OPAL Collaboration, G. Abbiendi et al., Eur. Phys. J. C **17**, 373 (2000)
99. OPAL Collaboration, R. Akers et al., Z. Phys. C **63**, 181 (1994)
100. ALEPH Collaboration, R. Barate et al., Eur. Phys. J. C **5**, 205 (1998)
101. DELPHI Collaboration, P. Abreu et al., Eur. Phys. J. C **5**, 585 (1998)
102. SLD Collaboration, K. Abe et al., Phys. Rev. D **59**, 052001 (1999)
103. DELPHI Collaboration, P. Abreu et al., Z. Phys. C **65**, 587 (1995)
104. ALEPH Collaboration, R. Barate et al., Phys. Rep. **294**, 1 (1998)
105. ALEPH Collaboration, R. Barate et al., Eur. Phys. J. C **16**, 613 (2000)
106. ALEPH Collaboration, A. Heister et al., Phys. Lett. B **528**, 19 (2002)
107. DELPHI Collaboration, P. Abreu et al., Phys. Lett. B **449**, 364 (1999)
108. ALEPH Collaboration, W. Krebs, ALEPH-99-057
109. OPAL Collaboration, K. Ackerstaff et al., Eur. Phys. J. C **5**, 411 (1998)
110. L3 Collaboration, M. Acciarri et al., Phys. Lett. B **393**, 465 (1997)
111. OPAL Collaboration, P.D. Acton et al., Phys. Lett. B **305**, 407 (1993)
112. OPAL Collaboration, R. Akers et al., Z. Phys. C **68**, 1 (1995)
113. DELPHI Collaboration, P. Abreu et al., Z. Phys. C **73**, 61 (1996)
114. OPAL Collaboration, K. Ackerstaff et al., Eur. Phys. J. C **4**, 19 (1998)
115. DELPHI Collaboration, P. Abreu et al., Phys. Lett. B **318**, 249 (1993)
116. OPAL Collaboration, G. Alexander et al., Z. Phys. C **73**, 569 (1997)
117. DELPHI Collaboration, P. Abreu et al., Z. Phys. C **67**, 543 (1995)
118. OPAL Collaboration, G. Alexander et al., Z. Phys. C **73**, 587 (1997)
119. L3 Collaboration, M. Acciarri et al., Phys. Lett. B **479**, 79 (2000)
120. DELPHI Collaboration, W. Adam et al., Z. Phys. C **70**, 371 (1996)
121. DELPHI Collaboration, P. Abreu et al., Phys. Lett. B **475**, 429 (2000)
122. DELPHI Collaboration, P. Abreu et al., Phys. Lett. B **361**, 207 (1995)
123. OPAL Collaboration, G. Alexander et al., Phys. Lett. B **358**, 162 (1995)
124. DELPHI Collaboration, J. Abdallah et al., Phys. Lett. B **569**, 129 (2003)
125. DELPHI Collaboration, P. Abreu et al., Eur. Phys. J. C **18**, 203 (2000); Erratum: Eur. Phys. J. C **25** (2002) 493.